

# Flavor sensitivity to $\theta_{13}$ and $\text{sign}(\delta m_{32}^2)$ for neutrinos from solar WIMP annihilation

Ralf Lehnert<sup>1,\*</sup> and Thomas J. Weiler<sup>2,†</sup>

<sup>1</sup>*Instituto de Ciencias Nucleares, Universidad Nacional Autónoma de México, A. Postal 70-543, 04510 México D.F., Mexico*

<sup>2</sup>*Department of Physics and Astronomy, Vanderbilt University, Nashville, TN 37235, USA*

(Dated: February 11, 2010)

The effect of the higher-energy 2nd resonance and the associated adiabatic-to-nonadiabatic transition on neutrino propagation in solar matter is presented. For WIMP-annihilation neutrinos injected with energies in the “sweet region” between 300 MeV and 10 GeV at the Sun’s center, a significant and revealing dependence on the neutrino mass hierarchy and the mixing angle  $\theta_{13}$  down to  $0.5^\circ$  is found in the flavor ratios arriving at Earth. In addition, the amplification of flavor ratios in the sweet region allows a better discrimination among possible annihilation modes of the solar dark matter. Under mild assumptions on WIMP properties, it is estimated that 200 neutrino events in the sweet region would be required for inferences of  $\theta_{13}$ , the mass hierarchy, and the dominant WIMP annihilation mode. Future large-volume, low-energy neutrino detectors are likely needed if the measurement is to be made.

PACS numbers: 14.60.Pq, 95.85.Ry, 26.65.+t, 95.35.+d

## I. INTRODUCTION

The annihilation of weakly interacting massive particles (WIMPs), trapped in the Sun’s core, is expected to produce fluxes of neutrinos and antineutrinos of all active flavors at energies well above the MeV scale of solar-fusion  $\nu_e$ ’s. These WIMP-annihilation neutrinos encounter the 2nd matter resonance at higher energy  $E_R^h \simeq |\delta m_{32}^2| \cos 2\theta_{13} / [2 V_e(0)] \sim 0.2$  GeV. We find that a small leptonic mixing angle  $\theta_{13}$  will inject a tell-tale signal in the flavor spectrum at Earth in the energy region 0.3–10 GeV, much as the 1st resonance at lower energy  $E_R^l \simeq \delta m_{21}^2 \cos 2\theta_{12} / [2 V_e(0) \cos^2 \theta_{13}] \sim 1.8$  MeV is expected to do in future measurements of the solar-fusion  $\nu_e$  spectrum. This signal implies an experimental sensitivity to  $\theta_{13}$ , presently constrained by CHOOZ data to be below  $12^\circ$ , down to about half a degree. In the above expressions,  $\delta m_{jk}^2 \equiv m_j^2 - m_k^2$ , and  $V_e(0) \sim 7 \times 10^{-12}$  eV is the matter potential resulting from the electron density at the Sun’s core; the superscripts  $h$  and  $l$  denote the higher-energy 2nd resonance and the lower-energy 1st resonance, respectively. The signal comes from the adiabatic-to-nonadiabatic transition at the 2nd resonance. This effect is the higher-energy boundary of the “bathtub” spectral shape, well-known and well-described for the 1st solar resonance, and elucidated for the 2nd solar resonance in Figs. 3 and 4 of Ref. [1] as well as herein.

The Borexino experiment [2] in progress and the SNO+ experiment [3] in the construction stage are likely to measure the  ${}^7\text{Be}$  and  $pep$  monochromatic solar neutrinos at energies of 0.861 MeV and 1.442 MeV, respectively. These measurements should reveal the lower-energy boundary of the bathtub profile from the 1st resonance. The adiabatic-to-nonadiabatic transition at the

2nd resonance offers a potentially much more striking signal than the lower-energy resonance, as we will show in the present work. The heuristic reason is that MSW resonant enhancement of the small  $\theta_{13}$  to the MSW resonant value of  $45^\circ$  is a much larger effect than the enhancement of  $\theta_{12} \sim 32^\circ$  to the resonant  $45^\circ$  value. In fact, as we will demonstrate, the adiabatic-to-nonadiabatic transition at the 2nd resonance is extremely sensitive to the value of small  $\theta_{13}$ : the resonance is completely nonadiabatic and ignorable for  $\theta_{13} = 0$ , whereas the adiabatic component is significantly amplified for nonzero  $\theta_{13}$ , even as small as  $0.5^\circ$ . In addition, the 2nd resonance occurs in the neutrino sector if the neutrino mass hierarchy is normal (i.e.,  $\delta m_{32}^2 > 0$ ), but in the antineutrino sector if the mass hierarchy is inverted (i.e.,  $\delta m_{32}^2 < 0$ ). WIMP annihilation in the Sun is expected to produce neutrinos and antineutrinos in equal numbers. The different absorption and scattering cross-sections of neutrinos versus antineutrinos in terrestrial detectors then allows possible discrimination between the two. It thus becomes apparent that the 2nd resonance provides the potential to reveal not only the value of  $\theta_{13}$ , but also the neutrino mass hierarchy codified as  $\text{sign}(\delta m_{32}^2)$ .

As in the case of solar-fusion neutrinos, the total neutrino spectrum remains unaffected by the resonance structure [4]. It is rather the distribution of the neutrinos over the three flavors that depends on the resonance physics. For this reason, we focus our attention on the individual flavor spectra (three flavors each for neutrinos and antineutrinos) that experiments at Earth can, in principle, detect.

While much theoretical effort has gone into studies of “indirect detection” of solar WIMPs by identification of their high-energy neutrino flux in large terrestrial detectors [5], little has been done [1, 6] to elucidate the possibilities at lower energies,  $E \lesssim 10$  GeV. The reasons are clear: most of the neutrino flux from WIMP annihilation is expected to populate the higher-energy region, the atmospheric background falls as  $\sim E^{-3}$  above

\*Electronic mail: ralf.lehnert@nucleares.unam.mx

†Electronic mail: tom.weiler@vanderbilt.edu

10 GeV [7], and the detection cross section for a neutrino grows as  $\sim E$  above GeV neutrino energies. However, the substantial discovery potential that hides in the solar WIMP-annihilation neutrino data below 10 GeV compels us to promote the associated lower-energy physics. In the next section, we present an overview of this rich neutrino physics at lower energies. Details, drawn mainly from Ref. [1], are presented in subsequent sections.

## II. PRELIMINARIES AND OVERVIEW

A statistical average over the oscillation phase  $\phi = \delta m_{jk}^2 L/2E$  effectively results from the uncertainties in the baseline  $L$  and energy  $E$  of solar neutrinos. The production flavor ratios  $w_\alpha(E)$  in the Sun’s core and the terrestrial flavor ratios  $W_\alpha(E)$  for neutrinos are then related by [1]:

$$\begin{pmatrix} W_e \\ W_\mu \\ W_\tau \end{pmatrix} = \underline{U} \underline{P} \underline{U}_m^T(r=0) \begin{pmatrix} w_e \\ w_\mu \\ w_\tau \end{pmatrix}. \quad (1)$$

Here,  $(\underline{U}_m)_{\alpha j} \equiv |(U_m)_{\alpha j}|^2$  is a classical probability matrix, constructed from the mixing matrix in matter  $U_m$ . The transposed matrix  $\underline{U}_m^T(r)$  transforms the production flavor fluxes to the propagating mass-state fluxes. The argument  $r=0$  in Eq. (1) reminds us that WIMP annihilation occurs in the solar core, and so it is the matter density at the Sun’s center that determines  $\underline{U}_m^T(0)$ .

Possible nonadiabatic transitions between the effective-mass states at the 1st and 2nd resonances and other solar-matter effects are described by the level-crossing probability matrix  $\underline{P}$  [8–10]. Finally, the matrix  $\underline{U}_{\alpha j} \equiv |U_{\alpha j}|^2$ , determined from the usual vacuum mixing matrix  $U$ , transforms the mass states back to detectable flavor fluxes at Earth. Explicit expressions for  $U_m$  and  $\underline{P}$  in terms of neutrino energy  $E$ , solar-model coefficients, and neutrino parameters, as well as the analogous result for antineutrinos can be found in Ref. [1], along with many other relevant details. Some related references that study flavor issues for solar neutrinos arising from WIMP annihilation are listed in Ref. [11].

Inspection of Eq. (1) reveals that structures in the flavor spectra can potentially arise from three energy-dependent sources: the initial flavor ratios  $w_\alpha(E)$ , the mixing matrix in matter  $\underline{U}_m(r=0, E)$ , and the jump-probability matrix  $\underline{P}(E)$ . The vacuum mixing matrix  $U$ , and thus  $\underline{U}$ , are each independent of the neutrino energy, and so  $\underline{U}$  does not contribute to energy-dependent features in the terrestrial flavor spectra.

The first of the above sources for features in the terrestrial flavor spectra, namely  $w_\alpha$ , is WIMP-model dependent. A description of this energy dependence requires knowledge of the  $WIMP \rightarrow \nu_\alpha$  annihilation chains. Three possible decay chains are commonly invoked. They are neutrino production via decay of the intermediate states  $W^+W^-$ ,  $b\bar{b}$ , and  $\tau^+\tau^-$ . The latter two chains lead to

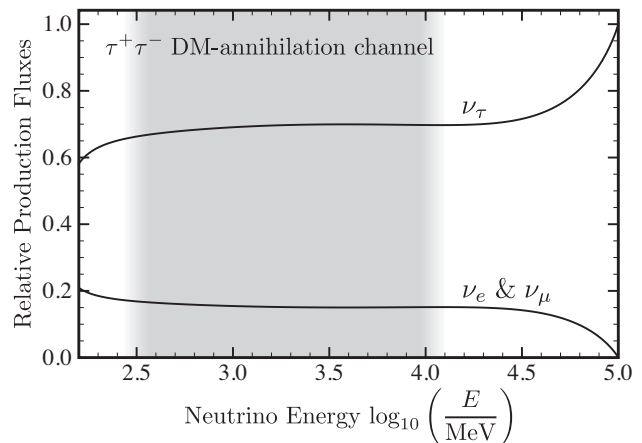


FIG. 1: Shown are the relative neutrino flavor spectra resulting from annihilation of WIMPs with 100 GeV mass into predominantly  $\tau^+\tau^-$ . This plot is based on the numerical results obtained by Cirelli *et al.* [12]. The shaded area represents the “sweet region” defined in the text. Note the nearly constant values of the relative fluxes inside this region.

softer neutrino spectra than does the former. Calculations [12] reveal that for the  $b\bar{b}$  and  $\tau^+\tau^-$  annihilation chains, the neutrino flavor ratios at production are slowly varying in the low-energy region [13]. For the  $W^+W^-$  chain, these flavor ratios are more energy-dependent [14]. We show the nearly energy-independent neutrino flavor spectra for  $M_{WIMP} = 100$  GeV annihilation via the  $\tau^+\tau^-$  mode in Fig. 1. For a 100 GeV WIMP mass, the region of nearly constant flavor ratios lies below 20–30 GeV [15]. For specificity in the rest of this paper, we will continue to focus on the  $b\bar{b}$  and (especially)  $\tau^+\tau^-$  modes, as well as on a WIMP mass of order 100 GeV. If the dominant annihilation mode of the WIMP is  $W^+W^-$  rather than  $\tau^+\tau^-$  and/or  $b\bar{b}$ , then we expect that the resonant flavor change that we describe below can still be extracted from data, but further efforts would be required to isolate the resonant features from the non-resonant energy-varying flavor ratios.

The second potential source of energy dependence, the matrix  $\underline{U}_m$ , can also be tamed: for neutrino energies sufficiently above the 2nd resonance,  $\underline{U}_m$  approaches an  $E$ -independent constant matrix (see e.g., Ref. [1]). For this reason, we will consider only energies well above  $E_R^h \sim 0.3$  GeV, so that  $\underline{U}_m$  is effectively constant.

Some energy dependence will also be introduced in the flavor ratios by the adiabatic-to-nonadiabatic transition of the 1st resonance. This occurs at energies at and above  $E_{NA}^l \sim 10$  GeV [1]. As can be seen in Figs. 3 and 4 of Ref. [1], the effects of the 1st resonance are mild; to ignore these effects would introduce little uncertainty into our calculation, and the effects could be included in a more complete analysis. However, we will simply restrict our study to energies below  $E_{NA}^l$  to shield our analysis from “contamination” due to the 1st resonance. Thus, we arrive at, and define, a “sweet region” in energy for

our analysis:

$$0.3 \text{ GeV} \leq E \leq 10 \text{ GeV} \quad \text{“SWEET REGION.”} \quad (2)$$

The results presented below will hold within this special region of energy.

The remaining and most important source of structure in the flavor spectra arises from the neutrino level-crossing probabilities at the resonances, which are described by the jump matrix  $\underline{P}$ . The transition from the adiabatic (i.e., no level-crossing) to the nonadiabatic (i.e., complete level-crossing) regime at high energies can leave a dramatic imprint in the terrestrial flavor-flux ratios.

In Ref. [1], the energy  $E_{NA}^h$  characterizing the onset of this adiabatic-to-nonadiabatic transition was defined implicitly by setting  $P_c^h(E_{NA}^h)$  in the crossing-probability matrix to  $e^{-3} \simeq 5\%$ . Numerically, this onset energy is  $E_{NA}^h \simeq 750 \sin^2 \theta_{13} \text{ GeV}$ . (An expression for the crossing probability is given below in Eq. (13).) The 2nd resonance occurs in the neutrino sector for the normal hierarchy with  $\delta m_{32}^2 > 0$ , and in the antineutrino sector for the inverted hierarchy with  $\delta m_{32}^2 < 0$ .

The above discussion shows that we may identify any observable energy dependence of the flavor spectra in the sweet region as due to the adiabatic-to-nonadiabatic transition at  $E_{NA}^h$ . In turn, the energy dependence in this sweet region will implicate the value of a small but nonzero  $\theta_{13}$  as well as the neutrino mass hierarchy. In particular, at small  $\theta_{13}$  the nonadiabatic jump probability is  $\exp(-\Gamma \theta_{13}^2)$ . The “adiabaticity parameter”  $\Gamma$  can be written in terms of the length scale  $\lambda_\odot = |\frac{d}{dr} \ln N_e|^{-1}$  for the change in the electron density  $N_e$  at the resonance region (corresponding to one  $e$ -folding in density for an exponential profile like that of the Sun), and the neutrino oscillation length in vacuum  $\lambda_\nu = 4\pi E/\delta m^2$  as  $\Gamma = 4\pi^2 \lambda_\odot/\lambda_\nu$ . The important feature for our purposes is that  $\Gamma$  scales as  $1/E$  and is therefore large, roughly 300–10 000, across the low energies of our sweet region. It is this large size of  $\Gamma$  that produces an observable signal even for extremely small  $\theta_{13}$ . Qualitatively, we expect sensitivity to  $\theta_{13}$  in the sweet region for  $\theta_{13}$  as small as  $1/\sqrt{\Gamma} \gtrsim 10^{-2} \sim 0.5^\circ$ . In Sec. IV, we show quantitatively that this is indeed the case.

There is also a terrestrial source of energy dependence in the flavor ratios. This arises from matter effects for neutrinos and antineutrinos traversing the Earth. The effect has been well worked out in publications [16]; it is somewhat complicated (best addressed with a numerical code), and we will not include it in this paper. We do give here some general remarks [1] about the Earth matter effect that are relevant for our present purposes. The resonant energies in Earth related to the solar scale  $\delta m_{21}^2$  are below the sweet region (at  $\sim 25 \text{ MeV}$  and  $\sim 100 \text{ MeV}$  for the Earth’s core and mantle, respectively), while the resonant energies in Earth related to the atmospheric-scale  $\delta m_{32}^2$  fall right in the sweet region, at  $\sim 2 \text{ GeV}$  and  $\sim 10 \text{ GeV}$  for the Earth’s core and mantle, respectively. As with the solar resonance, for a normal mass hierarchy the relevant resonance in Earth occurs in the neutrino but

not the antineutrino sector. And again as with the solar resonance, for an inverted mass hierarchy the relevant resonance in Earth occurs in the antineutrino but not the neutrino sector. The resonant amplification can be quite large, but the effect can be mitigated by a resonant oscillation wavelength scaling like  $1/\theta_{13}$ . The requirement that at least a quarter of the oscillation length must lie within the Earth to “feel” the matter effects leads to a nadir-dependent condition on  $\theta_{13}$ . For a neutrino with zero nadir angle,  $\theta_{13} \gtrsim 0.5^\circ (E/\text{GeV})$  is required to feel the matter; for other nadir angles, larger values of  $\theta_{13}$  are required to feel the matter. In a more complete analysis involving real data, terrestrial-matter effects should then no longer be ignored.

It is worth remarking here what would change if the WIMP mass were, say, a TeV rather than the 100 GeV we have assumed [13]. Surely, the available phase space for the produced neutrinos is increased. Moreover, in Ref. [12] it is shown that the upper end of the neutrino energy spectrum scales linearly with the WIMP mass, tending to enlarge the energy region in which the flavor ratios are constant. However, the sweet region remains between 0.3 and 10 GeV because it is determined solely by the effects of solar matter on neutrino propagation. It follows that the phase space of the sweet region relative to the enlarged total phase space now represents a smaller fraction, so that less sweet-region neutrinos are available. More importantly, according to Eq. (3) the expected neutrino flux from WIMP annihilation in the Sun scales as  $M_{\text{WIMP}}^{-2}$ , and so would be down by an additional factor of 100 for annihilation of TeV WIMPs compared to 100 GeV WIMPs.

One must inevitably ask what event rate at Earth might be expected from solar WIMP annihilation to (anti)neutrinos in the sweet region, and what rate is needed to observe structure in the terrestrial flavor spectra. We attend to first of these questions in the next section, and discuss the requirement for statistical significance in our final Sec. VI.

### III. (ANTI)NEUTRINO FLUX FROM SOLAR WIMP ANNIHILATION

Theory suggests that the age of the Sun exceeds the equilibration time between solar capture of WIMPs and their subsequent annihilation in the Sun [17]. Consequently, the WIMP annihilation rate is given by half of the WIMP capture rate, where the “half” just reflects the fact that it takes two captures to enable one two-body annihilation. The WIMP capture rate by the Sun is given in Ref. [17]:

$$C_\odot \simeq 1.0 \times 10^{25} \mathcal{F} \text{ s}^{-1}, \quad (3)$$

where

$$\mathcal{F} = \left( \frac{\rho_{\text{WIMP}}}{0.3 \frac{\text{GeV}}{\text{cm}^3}} \right) \left( \frac{270 \frac{\text{km}}{\text{s}}}{v_{\text{WIMP}}} \right) \left( \frac{\sigma_{\text{WIMP}}}{3 \times 10^{-38} \text{cm}^2} \right) \left( \frac{100 \text{GeV}}{M_{\text{WIMP}}} \right)^2 \quad (4)$$

is a fiducial factor. Here,  $\sigma_{\text{WIMP}}$  and  $M_{\text{WIMP}}$  are the unknown WIMP–nucleon scattering cross section and mass, while  $\rho_{\text{WIMP}}$  and  $v_{\text{WIMP}}$  denote the density and rms velocity of the local WIMP population. Each parenthetical fraction displays typical values, except that the fiducial value shown for  $\sigma_{\text{WIMP}}$  is the present upper limit for the spin-dependent cross section [18, 19]; it must therefore be viewed as optimistic. The inverse quadratic dependence of the rate on the WIMP mass is easily understood: one factor arise from the conversion of WIMP mass density  $\rho_{\text{WIMP}}$  to number density, and the other factor is kinematic, reducing the capture efficiency when the beam and target masses are mismatched. The fiducial values for today’s local WIMP density and rms velocity serve as numerical guidelines, but in fact the integrated history of WIMP capture by the Sun over large look-back times may yield values that do not adhere to these guidelines.

The WIMP–nucleon cross section in Eq. (4) above is the sum of a spin-independent cross section and a spin-dependent cross section, each averaged over the target matter in the Sun’s core. Experiments on Earth that search directly for WIMPs typically use target materials with large nucleon number, and so are better suited to limit (or detect) the spin-independent cross section [20]. Direct-search limits on the spin-dependent cross section are five orders of magnitude weaker than the limits on the spin-independent cross section. Since the solar material is mainly hydrogen, solar capture of WIMPs is very sensitive to the spin-dependent cross section.

An experimental measurement of the solar neutrino flux from WIMP annihilation would bypass the theoretical uncertainties just listed. So far, experiments have yielded only upper limits on this flux inferred from final-state muons with energies above a GeV [18, 19]. It is interesting to note that the bounds on the spin-dependent WIMP cross section inferred from these experimental neutrino-flux constraints are stronger than the bounds coming from direct searches for WIMPs [21].

We continue by considering the mean multiplicity of neutrinos,  $\xi_\nu$ , produced per annihilating WIMP (not WIMP pair), a quantity we anticipate to be of order unity. We can then estimate the total neutrino flux at Earth [22]:

$$\int dE \frac{dN_\nu}{dE} \simeq \frac{C_\odot \xi_\nu}{4\pi (\text{AU})^2} \sim \frac{1.1 \times 10^5 \xi_\nu \mathcal{F}}{\text{yr} \cdot \text{cm}^2}. \quad (5)$$

The background from “atmospheric neutrinos,” i.e., the neutrinos resulting from the decay of charged pions produced by cosmic-ray interactions in our atmosphere, has been calculated by many groups with convergent results. A typical energy spectrum in the GeV region can be found in Ref. [7]. It approximately obeys

$1.2 \times 10^6 \left( \frac{E}{\text{GeV}} \right)^{-2.75} (\text{GeV} \cdot \text{yr} \cdot \text{cm}^2)^{-1}$  for  $(\nu_\mu + \bar{\nu}_\mu)$ ; the all-flavor flux would be about three times larger. The integrated all-flavor flux above a GeV is then about  $2 \times 10^6/\text{yr cm}^2$ , with the spectral-index factor nearly compensating the flavor factor. This background flux is roughly twenty times the maximally allowed solar WIMP neutrino flux. Moreover, the background flux has a flavor content that varies with direction on the sky. The down-coming atmospheric neutrinos will show the 1 : 2  $\nu_e$  to  $\nu_\mu$  flavor ratio characteristic of the complete pion decay chain, as the muon decay length at lower energies is shorter than its atmospheric height, and the neutrino pathlength is shorter than its vacuum oscillation length  $L_{\text{osc}} = 4\pi E/\delta m^2 \sim 1000 (E/\text{GeV}) \text{ km}$ . In contrast, the upcoming neutrinos will show a 1:1 flavor ratio, since half of the  $\nu_\mu$ ’s will have oscillated into  $\nu_\tau$ ’s. On the bright side, the solar fraction of solid angle on the sky is quite small, approximately  $[\pi (R_\odot/\text{AU})^2]/4\pi \sim 5.4 \times 10^{-6}$ . So one may hope that a cut favoring the direction to the Sun would greatly increase the signal-to-background ratio. However, the mean scattering angle for neutrinos below 10 GeV is large,  $\theta_{\text{scatt}} \sim 20^\circ \sqrt{10 \text{GeV}/E}$ . The 24-hour angular modulation expected in the solar signal will help reduce the unmodulated atmospheric background. In addition, there has been some recent discussion of possible very large detectors [23], and some development in directional reconstruction of neutrinos at lower energies [24, 25]. There have also been recent studies of using event topologies to achieve partial “statistical” separation of neutrino and antineutrino data samples [26].

Multiplying the solar WIMP neutrino flux by (i) the neutrino–nucleon cross section, by (ii) the target number of nucleons given by

$$N_N = 6.0 \times 10^{35} \left( \frac{M_{\text{target}}}{\text{megaton}} \right), \quad (6)$$

and by (iii) the fraction of incident neutrino flux in the sweet region  $\Delta E(\text{SR})$  from 0.3 to 10 GeV

$$f_\nu \equiv \frac{\int_{\Delta E(\text{SR})} d \ln E \frac{dN_\nu}{d \ln E}}{\int d \ln E \frac{dN_\nu}{d \ln E}}, \quad (7)$$

one obtains the event rate within the sweet energy region. For a 100 GeV WIMP mass, inspection of the theoretical neutrino spectra in Ref. [12] suggests a value  $\sim 20\%$  for  $f_\nu$ , the fraction of neutrino flux in the sweet region between 0.3 and 10 GeV. As a fiducial event rate, we therefore take

$$R = 140 \left( \frac{\sigma_{\nu N}(E)}{10^{-38} \text{cm}^2} \right) \left( \frac{M_{\text{target}}}{\text{megaton}} \right) \left( \frac{f_\nu}{20\%} \right) \frac{\xi_\nu \mathcal{F}}{\text{yr}}. \quad (8)$$

For some perspective on the 140 events per year, we may ask how many events per year are to be expected in a proton-decay experiment at a megaton detector. The present limits on the lifetime of protons to decay to various modes are typically  $10^{35} \text{ yr}$ . The nucleon number in

a megaton is  $10^{12} N_A = 6 \times 10^{35}$ . So the expected event rate is

$$R_{p^+ \text{ decay}} = 6 \left( \frac{10^{35} \text{ yr}}{\tau_p} \right) \left( \frac{M_{\text{detector}}}{\text{megaton}} \right) \text{ yr}^{-1}. \quad (9)$$

We see that the rates for detection of solar neutrinos in the sweet region from WIMP annihilation and for detection for proton decay are comparable (although the backgrounds are different).

#### IV. THEORETICAL FRAMEWORK

To proceed, we need explicit expressions for the neutrino flavor spectrum produced by WIMP annihilation in the Sun's core in the range 0.3–10 GeV. We begin by parameterizing the relative production fluxes  $w_\alpha$ . In many models, the dominant WIMP-annihilation channels are  $b\bar{b}$ ,  $\tau^+\tau^-$ , and  $W^+W^-$ . The neutrino spectrum from each channel has been calculated (see, e.g., Ref. [12]), but the branching ratios to these channels depend on the specific model. Fortunately, WIMP decay obeys  $w_e(E) = w_\mu(E)$  to a very good approximation [12]. Since the normalization  $w_e + w_\mu + w_\tau = 1$  holds at any energy, the parametrization of the relative flavor spectra at production requires just one WIMP-model-dependent function  $f_F(E)$ .

We define  $f_F$  operationally via  $w_e = w_\mu = \frac{1}{3} - f_F$  and  $w_\tau = \frac{1}{3} + 2f_F$ . Positivity of the  $w_\alpha$  then implies the bound  $-\frac{1}{6} \leq f_F \leq +\frac{1}{3}$ . As defined,  $f_F$  is the deficit of  $w_e$  or  $w_\mu$  from  $\frac{1}{3}$  at injection in the solar core. Since maximal mixing effects symmetrization of  $\nu_\mu$  and  $\nu_\tau$ , it is also useful to view  $f_F$  as the excess of  $w_\nu \equiv w_\mu + w_\tau$  from  $\frac{2}{3}$ . To order  $f_F^2$ , the ratios  $(w_e/w_\tau)$  and  $(w_\mu/w_\tau)$  at injection are  $1 - 9f_F + 36f_F^2$ .

For comparative purposes later, it is also useful interpret  $f_F$  in terms of the evolved flavor probabilities  $W_\alpha$  in the *absence* of matter effects. The flavor density matrix at injection, in the flavor basis, is given by

$$\rho_F = \frac{1}{3} \mathbf{1} + f_F [2|\nu_\tau\rangle\langle\nu_\tau| - |\nu_\mu\rangle\langle\nu_\mu| - |\nu_e\rangle\langle\nu_e|]. \quad (10)$$

Using the tribimaximal mixing values to write this in the mass basis, and invoking phase averaging to remove the off-diagonal elements, one is left with just

$$\rho_F = \frac{1}{3} \mathbf{1} + \frac{1}{2} f_F [|\nu_3\rangle\langle\nu_3| - |\nu_1\rangle\langle\nu_1|]. \quad (11)$$

Then, the relative flavor probabilities  $W_\alpha$  are just  $\langle\nu_\alpha|\rho_F|\nu_\alpha\rangle$ . The results for vacuum transitions are  $W_e = \overline{W}_e = \frac{1}{3} - \frac{1}{3}f_F$ , and  $W_\mu = W_\tau = \overline{W}_\mu = \overline{W}_\tau = \frac{1}{3} + \frac{1}{6}f_F$ . The vacuum value for the ratios  $W_\mu/W_e$  and  $\overline{W}_\mu/\overline{W}_e$  to order  $f_F^2$  are  $1 + \frac{3}{2}f_F + f_F^2$ .

Although actual WIMP properties are unknown, we may consider two of the aforementioned annihilation channels,  $b\bar{b}$  and  $\tau^+\tau^-$ , as generic examples. We have

TABLE I: Values of  $f_F = \frac{1}{3} - w_e = \frac{1}{3} - w_\mu = \frac{1}{2}(w_\tau - \frac{1}{3})$  in the sweet region for popular WIMP annihilation modes.

WIMP annihilation mode	$f_F$ (sweet region)
$\tau^+\tau^-$	$+0.182 \pm 0.001$
$b\bar{b}$	$-0.09 \pm 0.01$
Higgs-like	$-0.07 \pm 0.01$
$W^+W^-$	$-0.029 + 0.014 (E/\text{GeV})$

argued that in our sweet region, the function  $f_F(E)$  is reduced to an energy-independent number  $f_F$  for the  $\tau^+\tau^-$  and  $b\bar{b}$  annihilation modes of the solar WIMPs. Our fitted values for  $f_F$  in these channels are  $-0.09 \pm 0.01$  and  $+0.182 \pm 0.001$ , respectively.

It is worth mentioning that in some WIMP models the annihilation to fermions proceeds through Higgs-like couplings. We then expect the  $b\bar{b}$  mode to dominate, but also a branching fraction to  $\tau^+\tau^-$  given by  $(m_\tau/m_b)^2/3 \sim 5\%$ , where the  $\frac{1}{3}$  reflects the  $b\bar{b}$  mode's color factor. In the sweet region, the  $f_F$ 's for the  $b\bar{b}$  and  $\tau^+\tau^-$  modes have opposite signs, so the *average*  $f_F$  for the fermionic channel is smaller in magnitude than  $f_F(b\bar{b})$  and  $f_F(\tau^+\tau^-)$ . However, the  $b\bar{b}$  mode, and thus its concomitant  $f_F$  value, dominate: an estimate employing the injection spectra given in Ref. [12] indeed yields  $f_F(\text{Higgs}) \simeq -0.07 \pm 0.01$  in proximity to the  $-0.09$  value for  $b\bar{b}$  mode. We remark that the neutrino spectrum from the  $\tau^+\tau^-$  mode is harder than that from the  $b\bar{b}$  mode, and at energies above the sweet region, of no relevance to the present paper, the  $\tau^+\tau^-$  mode becomes increasingly important and eventually comes to dominate. For the  $W^+W^-$  mode,  $f_F$  behaves quite differently: it rises nearly linearly with energy in the sweet region:  $f_F(W^+W^-) = -0.029 + 0.014 (E/\text{GeV})$ . The values for the various  $f_F$ 's presented in this paragraph have been estimated using the results in Ref. [12]; they are also collected in Table I.

We note that for equal initial flavors ( $f_F=0$ ), the resulting terrestrial flavor ratios are also democratic [1], i.e.,  $W_e = W_\mu = W_\tau = 1/3$ . This is most easily seen by noting that the commutator in the density-matrix evolution equation  $i \frac{d\rho}{dt} = [H, \rho]$  vanishes for  $\rho$  proportional to the identity matrix regardless of whether  $H$  is the vacuum or matter Hamiltonian. Thus, it is only the order 7–18%  $f_F$ -value differences in the initial flavor spectrum that evolve nontrivially. If flavor differences were not amplified by intervening matter effects, an event sample of about  $(n/15\%)^2$  would be necessary to yield an  $n$ -sigma statistical inference of this difference. However, we will see shortly that matter effects, quadratically sensitive to  $\theta_{13}$  and to the neutrino mass hierarchy, may amplify the flavor difference considerably.

For further progress, we also need explicit expressions for  $\underline{U}$ ,  $\underline{P}$ , and  $\underline{U}_m$  appearing in Eq. (1). In the sweet

TABLE II: Leading-order contributions to the components of the  $A$  and  $B$  flavor vectors in Eq. (12).

type	$e$ flavor	$\mu$ flavor	$\tau$ flavor
$A_\alpha^{\text{NH}}$	$2 + 4\delta\theta_{23}$	$-1 - 8\delta\theta_{23}$	$-1 + 4\delta\theta_{23}$
$B_\alpha^{\text{NH}}$	$-2 - 4\sqrt{2}\delta\theta_{12} + 4\delta\theta_{23}$	$1 + \sqrt{8}\delta\theta_{12} + 8\delta\theta_{23} + \sqrt{8}\theta_{13}\cos\delta$	$1 + \sqrt{8}\delta\theta_{12} - 12\delta\theta_{23} - \sqrt{8}\theta_{13}\cos\delta$
$\bar{A}_\alpha^{\text{NH}}$	$-2 + 4\sqrt{2}\delta\theta_{12} + 4\delta\theta_{23}$	$1 - \sqrt{8}\delta\theta_{12} - \sqrt{8}\theta_{13}\cos\delta$	$1 - \sqrt{8}\delta\theta_{12} + \sqrt{8}\theta_{13}\cos\delta - 4\delta\theta_{23}$
$\bar{B}_\alpha^{\text{NH}}$	0	0	0
$A_\alpha^{\text{IH}}$	$-4\sqrt{2}\delta\theta_{12} + 8\delta\theta_{23}$	$\sqrt{8}\delta\theta_{12} + \sqrt{8}\theta_{13}\cos\delta$	$\sqrt{8}\delta\theta_{12} - \sqrt{8}\theta_{13}\cos\delta - 8\delta\theta_{23}$
$B_\alpha^{\text{IH}}$	0	0	0
$\bar{A}_\alpha^{\text{IH}}$	$2 - 4\delta\theta_{23}$	$-1 - 4\delta\theta_{23}$	$-1 + 8\delta\theta_{23}$
$\bar{B}_\alpha^{\text{IH}}$	$-4 + 4\sqrt{2}\delta\theta_{12} + 8\delta\theta_{23}$	$2 - \sqrt{8}\delta\theta_{12} + 4\delta\theta_{23} - \sqrt{8}\theta_{13}\cos\delta$	$2 - \sqrt{8}\delta\theta_{12} - 12\delta\theta_{23} + \sqrt{8}\theta_{13}\cos\delta$

region, the level-crossing probability at the lower resonance is zero, as explained above. The fact that Eq. (1) is linear in the level-crossing probability matrix  $\underline{P}$  allows one to write a simple equation for the flavor evolution,

$$W_\alpha = \frac{1}{3} + \frac{1}{4} [A_\alpha + B_\alpha P_c^h(E)] f_F, \quad (12)$$

valid in the sweet region. The pre-factor of  $\frac{1}{4}$  in front of the square brackets is chosen for convenience. The flavor-indexed quantities  $A_\alpha$  and  $B_\alpha$ ,  $\alpha = e, \mu, \tau$ , are determined by the neutrino mixing parameters at the Sun's core (where  $\nu_e \sim \nu_3$ ) and at Earth (vacuum values) [27]. Since the mixing parameters are energy independent in the sweet region, so too are  $A_\alpha$  and  $B_\alpha$ . The flavor-vectors  $B_\alpha$  and  $A_\alpha$  do depend on the neutrino mass hierarchy and on incident neutrino versus antineutrino. Importantly, the entire energy dependence in the evolution equation (12) is contained in the level-crossing probability  $P_c^h(E)$  at the 2nd resonance, given by the expression

$$P_c^h(E) = \Theta(E - E_R^h) \frac{\exp(-\Gamma \sin^2 \theta_{13}) - \exp(-\Gamma)}{1 - \exp(-\Gamma)} \\ \simeq \exp(-\Gamma \sin^2 \theta_{13}). \quad (13)$$

In this expression,  $\Theta$  denotes the unit-step function, and  $\mathcal{O}(\delta m_{21}^2/|\delta m_{32}^2|) \sim 0.03$  terms have been dropped. As mentioned in the overview section, the adiabaticity parameter  $\Gamma$  may be written as

$$\Gamma = 4\pi^2 \frac{\lambda_\odot}{\lambda_v}, \quad (14)$$

where

$$\lambda_\odot \equiv \left| \frac{d}{dr} \ln N_e(r) \right|^{-1} \quad (15)$$

is the scale of density change (the distance for an  $e$ -folding change in the solar density, equal to  $6.6 \times 10^4$  km) and  $\lambda_v \equiv 4\pi E/\delta m_{32}^2$  is the oscillation length in vacuum. Consequently,  $\Gamma$  scales as  $1/E$ , and we define a constant  $\tilde{\Gamma}$  via

$$\Gamma \equiv \frac{\tilde{\Gamma}}{E}, \quad (16)$$

where

$$\tilde{\Gamma} \simeq 2.5 \times \left( \frac{|\delta m_{32}^2|}{2.5 \times 10^{-3} \text{ eV}^2} \right) \text{ TeV}, \quad (17)$$

for the higher-energy resonance in solar matter. With Eqs. (14)–(17) at hand, it is apparent that  $\Gamma \gtrsim 300$ . This large  $\Gamma$  value, together with the experimental input  $\sin^2 \theta_{13} \ll 1$  and the fact that  $E > E_R^h$  in the sweet region, has been used to obtain the second line of Eq. (13).

Note that the only neutrino mixing parameter contained in  $P_c^h(E)$  is  $\theta_{13}$ , and it enters essentially squared in an exponent. It follows then, that the dominant energy dependence of the terrestrial flavor ratios in the sweet region is governed by  $\theta_{13}$ , as advertised in the introduction. Moreover, the sensitivity of flavor evolution through the adiabatic-to-nonadiabatic transition is exponentially sensitive to  $\theta_{13}^2$ .

From Eqs. (13) and (16), we infer the onset energy for  $E_{NA}^h$  for the adiabatic-to-nonadiabatic transition to be

$$E_{NA}^h \equiv \frac{1}{3} \tilde{\Gamma} \sin^2 \theta_{13} \\ = 800 \sin^2 \theta_{13} \left( \frac{|\delta m_{32}^2|}{2.5 \times 10^{-3} \text{ eV}^2} \right) \text{ GeV}. \quad (18)$$

Neutrinos with energy  $E_R^h < E \lesssim E_{NA}^h$  will experience adiabatic level-repulsion at the 2nd resonance, whereas neutrinos with  $E \gg E_{NA}^h$  will experience nonadiabatic level-crossing at the 2nd resonance. We remark that although it is true in the Sun that the adiabatic-to-nonadiabatic transition energy  $E_{NA}^h$  exceeds the resonant energy  $E_R^h$ , this ordering is not in general guaranteed. The ratio of the two energies is

$$\frac{E_{NA}^h}{E_R^h} = \frac{2\pi \sin^2 \theta_{13}}{3 \cos 2\theta_{13}} \left[ \frac{\sqrt{2} G_F N_e}{\left| \frac{d}{dr} \ln N_e \right|} \approx \sqrt{2} G_F \lambda_\odot N_e(0) \right]. \quad (19)$$

Numerically, the term in brackets is 1800 for the Sun. It is this fortuitously large value for the Sun that allows the adiabatic-to-nonadiabatic transition to probe  $\theta_{13}$  values all the way down to  $\theta_{13} \sim (\frac{2\pi}{3} 1800)^{-\frac{1}{2}} \sim 1^\circ$ .

We proceed by defining the energy  $E_{1/2}$  at which the crossing probability is one half. From Eqs. (13) and (16) we readily find that

$$E_{1/2} = \frac{\tilde{\Gamma} \sin^2 \theta_{13}}{\ln 2} = 3.6 \sin^2 \theta_{13} \left( \frac{|\delta m_{32}^2|}{2.5 \times 10^{-3} \text{ eV}^2} \right) \text{ TeV}. \quad (20)$$

Let us also define the width of the change in crossing probability as  $\Delta E = E_+ - E_-$ , where  $P_c^h(E_-) = 1/e$  and  $P_c^h(E_+) = 1 - 1/e$ . This yields

$$\Delta E = (e - 1) (\ln 2) E_{1/2} \simeq 1.19 E_{1/2}. \quad (21)$$

It is seen that  $E_{1/2}$  as well as  $\Delta E$  are approximately equal to  $4 \sin^2 \theta_{13} \approx 4 \theta_{13}^2$  in units of TeV. Both  $E_{1/2}$  and  $\Delta E$  are very sensitive probes of the unknown  $\theta_{13}$ . The experimental upper bound  $\sin \theta_{13} \leq 0.22$  at  $3\sigma$  establishes that  $\theta_{13} \simeq \sin \theta_{13}$  to better than 1% accuracy. Accordingly, we may invert Eq. (20) to obtain

$$\theta_{13} = 1.0^\circ \sqrt{\left( \frac{E_{1/2}}{\text{GeV}} \right) \left( \frac{2.5 \times 10^{-3} \text{ eV}^2}{|\delta m_{32}^2|} \right)}. \quad (22)$$

For  $\theta_{13}$  in the phenomenologically interesting range  $0.6^\circ \leq \theta_{13} \leq 3^\circ$ , Eq. (20) tells us that  $E_{1/2}$  lies within the sweet region. Then, the inverse Eq. (22) establishes that a measurement of the adiabatic-to-nonadiabatic transition energy, via changing flavor ratios, probes the  $\theta_{13}$  mixing angle in this very interesting range from  $0.6^\circ$  to  $3^\circ$ . Equation (22) is the most important result of this paper. We show below that the flavor signal is also sensitive to the neutrino mass hierarchy.

The ratio  $\Delta E/E_{1/2} \simeq 1.19$  is independent of  $\theta_{13}$ . Consequently, the number of events needed to establish  $E_{1/2}$ , and thereby  $\theta_{13}$ , is independent of  $\theta_{13}$  or  $E_{1/2}$ . Of course, the necessary event number will depend on the magnitude of flavor change over the transition region. Since  $\Delta E \sim E_{1/2}$ , we have that  $\Delta E/E = \Delta \ln E \sim 1$ . From this we infer that the relevant event sample must span about a natural log in energy about  $E_{1/2}$  to map out the transition region in detail, again independent of  $\theta_{13}$  or  $E_{1/2}$ . However, to measure the gross change in flavor ratios across the transition, an event sample may be drawn from an energy region as large as the entire sweet region, 0.3 to 10 GeV. The availability of this wide energy range for the data sample is fortunate, for at the relatively low energies of the sweet region, large uncertainties are expected in the reconstruction of the neutrino energy from the measured charged lepton.

The change in the flavor ratios across the adiabatic-to-nonadiabatic transition region of width  $\Delta E$  centered on  $E_{1/2}$  is the signal. The magnitude of the flavor change across the transition region is determined by Eq. (12) and depends on the parameters  $A_\alpha$  and  $B_\alpha$ . These parameters in turn depend on the neutrino mixing angles, the mass hierarchy, and the particle type (neutrinos vs. antineutrinos). The two hierarchies and the neutrino versus antineutrino type lead to four possibilities. To distinguish among these possibilities, we employ the notation

$A_\alpha^{\text{NH}}, \bar{A}_\alpha^{\text{IH}}$ , etc., where the bar denotes the antineutrino case and the superscripts NH and IH refer to the normal and inverted hierarchy, respectively. For our present purposes, it is sufficient to employ the ‘‘tribimaximal’’ values [28] for the two large mixing angles, i.e., to set  $\sin^2 \theta_{23}^{\text{TBM}} = 1/2$  and  $\sin^2 \theta_{12}^{\text{TBM}} = 1/3$ . The phenomenological accuracy of this approximation is very good, as is summarized in Ref. [29].

Although we employ the tribimaximal values for  $\theta_{32}$  and  $\theta_{12}$  in what follows, we nevertheless exhibit in Table II, for possible future use, the first-order corrections to the  $A_\alpha$  and  $B_\alpha$  that result if the neutrino mixing angles deviate from their tribimaximal values. To this end, we have denoted the deviations from the tribimaximal case by  $\delta\theta_{jk} \equiv \theta_{jk} - \theta_{jk}^{\text{TBM}}$ . The expressions in Table II result from a calculation paralleling that in Appendix D of Ref. [1]. The  $3\sigma$  experimental uncertainties in the angles are [30]

$$\begin{aligned} -10.4^\circ &\leq \delta\theta_{32} \leq 8.6^\circ, \\ -4.8^\circ &\leq \delta\theta_{21} \leq 4.0^\circ, \\ 0^\circ &\leq \theta_{13} \leq 12.9^\circ. \end{aligned} \quad (23)$$

Consequently, future data may mandate deviations from the tribimaximal-based  $A_\alpha$  and  $B_\alpha$  used in this work.

## V. RESULTS

In the first subsection, we present results valid to all orders in  $f_F$ . In particular, we provide figures for the  $\tau^+\tau^-$  annihilation mode generated with the complete energy dependence of  $f_F(E)$  over an energy range that includes the sweet region. In the second subsection, we present analytic formulas for the sweet region valid to order  $f_F^2$  and compare (favorably) their validity with the more exact figures.

### A. Exact results

The explicit expressions for the neutrino and antineutrino flavor ratios with the normal hierarchy are

$$\begin{aligned} W_e^{\text{NH}} &= \frac{1}{3} + \frac{1}{4} (2 - 2 P_c^h) f_F \\ W_{\mu/\tau}^{\text{NH}} &= \frac{1}{3} + \frac{1}{4} (-1 + [1 \pm \sqrt{8} \theta_{13} \cos \delta] P_c^h) f_F \\ \bar{W}_e^{\text{NH}} &= \frac{1}{3} + \frac{1}{4} (-2) f_F \\ \bar{W}_{\mu/\tau}^{\text{NH}} &= \frac{1}{3} + \frac{1}{4} (1 \mp \sqrt{8} \theta_{13} \cos \delta) f_F. \end{aligned} \quad (24)$$

The analogous expressions for the flavor ratios with the inverted hierarchy are

$$\begin{aligned}
W_e^{\text{IH}} &= \frac{1}{3} + 0 \cdot f_F & (25) \\
W_{\mu/\tau}^{\text{IH}} &= \frac{1}{3} \pm \frac{1}{4} (\sqrt{8} \theta_{13} \cos \delta) f_F \\
\overline{W}_e^{\text{IH}} &= \frac{1}{3} + \frac{1}{4} (2 - 4P_c^h) f_F \\
\overline{W}_{\mu/\tau}^{\text{IH}} &= \frac{1}{3} + \frac{1}{4} (-1 + [2 \mp \sqrt{8} \theta_{13} \cos \delta] P_c^h) f_F.
\end{aligned}$$

In these equations, the upper and lower signs refer to the  $\mu$  and  $\tau$  flavors, respectively. The resonance terms, proportional to  $P_c^h$ , appear where they should: in the neutrino sector for the NH, and in the antineutrino sector for the IH. Note also that in the nonadiabatic limit, i.e., with  $P_c^h$  set equal to one, the 2nd resonance becomes irrelevant and the NH and IH cases properly reduce to the same result. Note also that the asymmetry between neutrinos and antineutrinos is unsurprising: the solar medium contains no antimatter and in this sense provides a CPT-violating background [31].

In what follows, we will omit the small, explicit  $\theta_{13}$  dependence from Eqs. (24) and (25) for brevity, but we will of course retain the primary  $\theta_{13}$  dependence in  $P_c^h$  as given by Eq. (13). With  $\theta_{13}$  removed, the mixing is strictly tribimaximal, with its inherent  $\nu_\mu \leftrightarrow \nu_\tau$  interchange symmetry: the  $\pm$  signs in Eqs. (24) and (25), which differentiate  $\nu_\mu$  and  $\nu_\tau$ , disappear.

We now turn to the event types in the detector. A minority of the events will be neutral current (NC) events. NC events yield no flavor information, and we ignore them. The majority of events will be charged-current (CC) events producing a charged lepton. Among these CC events, we note that the threshold in energy for production of a charged  $\tau$  is  $m_\tau (1 + m_\tau/2 m_N) = 3.47$  GeV. Since this value falls in the middle of the sweet region, it presents a kinematic complication. It is therefore advantageous to consider observables that do not depend on CC  $\tau$  production. For this reason, we examine the ratios  $(W_\mu/W_e)$ ,  $(\overline{W}_\mu/\overline{W}_e)$ ,  $(\overline{W}_e/W_e)$ , and  $(\overline{W}_\mu/W_\mu)$ . The threshold for the muon CC is  $E = m_\mu (1 + m_\mu/2 m_N) = 110$  MeV, well below the lower end (300 MeV) of our sweet region. For experiments with charge identification, e.g., the proposed large magnetized iron INO experiment, these ratios may be inferred from measurements of  $\nu_\mu$  CC events, which necessarily contain a muon-track signature, as well as from  $\nu_e$  CC events, which necessarily contain an electromagnetic plus hadronic shower and no muon track. For experiments without charge identification, which can contain a much larger target mass, we must sum  $\nu$  and  $\bar{\nu}$  and work with the single ratio  $\mathcal{R} \equiv (W_\mu + \overline{W}_\mu)/(W_e + \overline{W}_e)$ .

In practice, there will be experimental efficiencies that differ significantly for the detection of neutrinos versus antineutrinos, and muon versus electron CC reactions. Among other sources of these efficiency differences are the unequal CC cross sections for scattering of  $\nu_\mu$  ver-

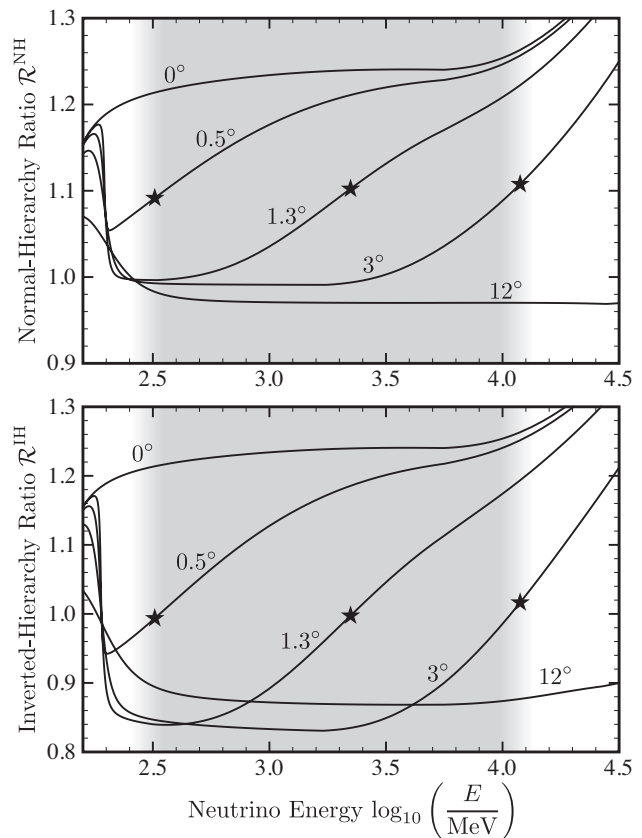


FIG. 2: The normal-hierarchy ratio  $\mathcal{R}^{\text{NH}} = (W_\mu^{\text{NH}} + \overline{W}_\mu^{\text{NH}})/(W_e^{\text{NH}} + \overline{W}_e^{\text{NH}})$  (top) and inverted-hierarchy ratio  $\mathcal{R}^{\text{IH}} = (W_\mu^{\text{IH}} + \overline{W}_\mu^{\text{IH}})/(W_e^{\text{IH}} + \overline{W}_e^{\text{IH}})$  (bottom) versus the neutrino energy  $E$  for the indicated  $\theta_{13}$  mixing angles. Here,  $M_{\text{WIMP}} = 100$  GeV, and the annihilation mode is assumed to be predominantly  $\tau^+\tau^-$ . The approximate location of the “sweet region,” where our analytical results apply, is shaded. The star ( $\star$ ) indicates the location of the energy  $E_{1/2}$  at which the crossing probability is one half. The neutrino mass-squared differences are  $\delta m_{21}^2 = 8.0 \times 10^{-5} \text{ eV}^2$  and  $\delta m_{32}^2 = \pm 3.0 \times 10^{-3} \text{ eV}^2$ ,  $\theta_{21}$  and  $\theta_{32}$  are given their tribimaximal values, and the CP-violating phase  $\delta$  is set to zero. The family of curves are quite sensitive to the value of  $\theta_{13}$ , even below a degree. Relative changes in  $\mathcal{R}$  are 20% for the normal hierarchy (top) and 30% for the inverted hierarchy (bottom), with the centered energy  $E_{1/2}$  showing quadratic sensitivity to  $\theta_{13}$  in agreement with Eq. (20). We remark that the non-trivial behavior just below the sweet region results primarily from the lower-energy resonance as well as from the energy dependence of  $U_m(E)$ .

sus  $\nu_e$  versus  $\bar{\nu}_\mu$  versus  $\bar{\nu}_e$ . Over the energy range of the sweet region, the nature of neutrino scattering is quite energy dependent. Relevant cross sections include inverse  $\beta$  decay, neutrino–electron scattering, quasi-elastic scattering, pion production, and deep inelastic scattering. We note that efficiency differences may be advantageous if they can mitigate the mixing of  $\nu_\mu$ ,  $\nu_e$ ,  $\bar{\nu}_\mu$ , and  $\bar{\nu}_e$  signals. However, in this work we will simply assume uniform efficiencies for detection of  $\nu_\mu$ ,  $\nu_e$ ,  $\bar{\nu}_\mu$ , and  $\bar{\nu}_e$ ,



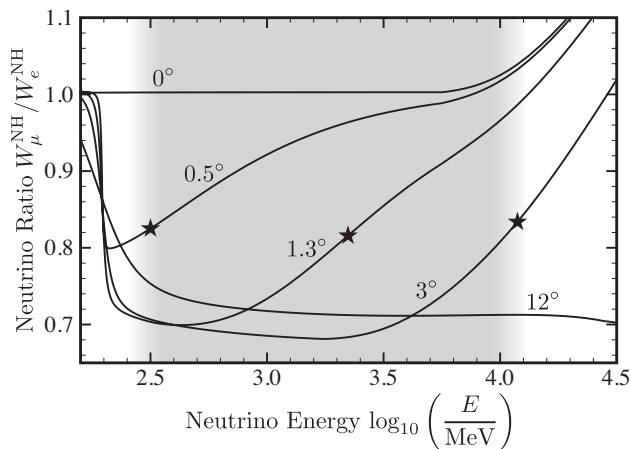


FIG. 3: The normal-hierarchy ratio  $W_\mu^{\text{NH}}/W_e^{\text{NH}}$  versus the neutrino energy  $E$  for various  $\theta_{13}$  mixing angles. Input parameters are identical to those in Fig. 2. The relative change in flavor ratio is about 40% across the transition region. Again,  $E_{1/2}$  (denoted by  $\star$ ) depends quadratically on  $\theta_{13}$ , allowing a potential inference of this mixing angle. In the normal hierarchy, the 2nd resonance occurs in the neutrino sector and not in the antineutrino sector.

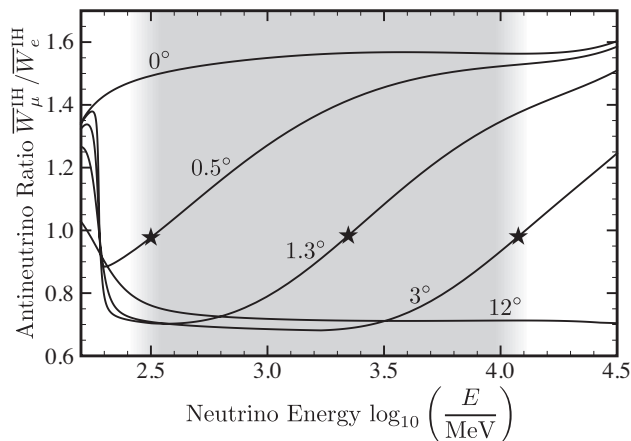


FIG. 4: The inverted-hierarchy ratio  $\overline{W}_\mu^{\text{IH}}/\overline{W}_e^{\text{IH}}$  versus the neutrino energy  $E$  for various  $\theta_{13}$  mixing angles. The input parameters are identical to those in Fig. 2. The relative change in flavor ratio is almost a factor of two across the transition region. Again,  $E_{1/2}$  (denoted by  $\star$ ) depends quadratically on  $\theta_{13}$  allowing a potential deduction of this mixing angle. In the inverted hierarchy, the 2nd resonance occurs in the antineutrino sector and not in the neutrino sector.

rather than introduce another layer of complexity.

The ratio  $\mathcal{R} = (W_\mu + \overline{W}_\mu)/(W_e + \overline{W}_e)$  is defined to weight equally the event numbers of neutrino and antineutrinos. Since the 2nd resonance occurs only in the neutrino sector (NH) or only in the antineutrino sector (IH), but not in both, the contribution of the non-resonant sector (neutrino or antineutrino) will mitigate the contribution from the resonant sector. In this sense,  $\mathcal{R}$  as defined is a conservative variable.

The energy dependence of the ratio  $\mathcal{R}$  is presented without approximation in Fig. 2. One sees that even for

this conservative variable, 20–30% changes in the relative flavor ratio occur across the adiabatic-to-nonadiabatic transition in the 0.3–10 GeV sweet region. Curves are parameterized by values of  $\theta_{13}$ , with significant effects apparent all the way down to a fraction of a degree. The quadratic dependence of  $E_{1/2}$  (defined as the energy where the nonadiabatic crossing probability is 50% and denoted in the figures by a  $\star$ ) on  $\theta_{13}$  is clearly seen. In favorable circumstances, this ultra-sensitivity of the spectrum to  $\theta_{13}$  could potentially be used to measure  $\theta_{13}$ .

Notable is that the change in the flavor ratio is about twice as large for the inverted neutrino mass hierarchy as it is for the normal hierarchy. We can dissect some of this behavior by turning to ratios defined only in the neutrino sector or only in the antineutrino sector. By excluding the non-resonant sector from the flavor ratio, we expect the change in the ratio across the adiabatic-to-nonadiabatic transition to be about twice that of the sector-summed result. That is, we expect  $\sim 40\%$  effects in the neutrino sector if the hierarchy is normal, and  $\sim 80\%$  effects in the antineutrino sector if the hierarchy is inverted. In Figs. 3 and 4, we see that this expectation is met. Consequently, if some experimental handle is available to even partially separate the neutrino and antineutrino data samples, then considerably greater discriminatory power becomes available. Put another way, across the sweet region, with the normal hierarchy, the neutrino flavor ratio should exhibit considerable energy dependence and the antineutrino flavor ratio should not. Conversely, with the inverted hierarchy, the antineutrino flavor ratio should show significant energy dependence and the neutrino flavor ratio should not. Thus, if neutrino–antineutrino discrimination becomes possible, then the observed energy dependence of neutrino versus antineutrino flavor ratios differentiates between the two possible mass hierarchies.

## B. Approximate results

With the exact evolved flavor relations of Eqs. (24) and (25) in hand, we may take ratios and expand in powers of the small  $f_F$ 's given in Table I. To order  $f_F^2$ , one finds for the normal hierarchy:

$$\mathcal{R}^{\text{NH}} = 1 + \frac{9}{8} P_c^h f_F + \frac{27}{32} (P_c^h)^2 f_F^2, \quad (26)$$

$$\left(\frac{W_\mu^{\text{NH}}}{W_e^{\text{NH}}}\right) = 1 - \frac{9}{4} (1 - P_c^h) f_F + \frac{27}{8} (1 - P_c^h)^2 f_F^2, \quad (27)$$

$$\left(\frac{\overline{W}_\mu^{\text{NH}}}{\overline{W}_e^{\text{NH}}}\right) = 1 + \frac{9}{4} f_F + \frac{27}{8} f_F^2, \quad (28)$$

$$\left(\frac{\overline{W}_e^{\text{NH}}}{W_e^{\text{NH}}}\right) = 1 - \frac{3}{2} (2 - P_c^h) f_F + \frac{9}{4} P_c^h (1 - P_c^h) f_F^2, \quad (29)$$

$$\left(\frac{\overline{W}_\mu^{\text{NH}}}{W_\mu^{\text{NH}}}\right) = 1 - \frac{3}{4} (2 - P_c^h) f_F + \frac{9}{16} P_c^h (1 - P_c^h) f_F^2. \quad (30)$$

These equations reflect the fact that with the normal hierarchy, the 2nd resonance and the adiabatic-to-nonadiabatic transition lie in the neutrino sector and not in the antineutrino sector.

The analogous calculation for the inverted hierarchy yields

$$\mathcal{R}^{\text{IH}} = 1 - \frac{9}{8}(1 - 2P_c^h) f_F - \frac{9}{32}(1 - 2P_c^h)^2 f_F^2, \quad (31)$$

$$\left(\frac{W_\mu^{\text{IH}}}{W_e^{\text{IH}}}\right) = 1 + 0 \cdot f_F + 0 \cdot f_F^2, \quad (32)$$

$$\left(\frac{\overline{W}_\mu^{\text{IH}}}{\overline{W}_e^{\text{IH}}}\right) = 1 - \frac{9}{4}(1 - 2P_c^h) f_F + \frac{27}{8}(1 - 2P_c^h)^2 f_F^2, \quad (33)$$

$$\left(\frac{\overline{W}_e^{\text{IH}}}{\overline{W}_e^{\text{IH}}}\right) = 1 + \frac{3}{2}(1 - 2P_c^h) f_F + 0 \cdot f_F^2, \quad (34)$$

$$\left(\frac{\overline{W}_\mu^{\text{IH}}}{\overline{W}_\mu^{\text{IH}}}\right) = 1 - \frac{3}{4}(1 - 2P_c^h) f_F + 0 \cdot f_F^2. \quad (35)$$

The equations here reflect the fact that with the inverted hierarchy, the 2nd resonance and the adiabatic-to-nonadiabatic transition lie in the antineutrino sector and not in the neutrino sector.

For comparison, we remind the reader that in the absence of matter, the analogous vacuum-evolved ratios are  $(W_\mu/W_e)_{\text{vacuum}} = (\overline{W}_\mu/\overline{W}_e)_{\text{vacuum}} = 1 + \frac{3}{2}f_F + f_F^2$ , as has been established in Sec. IV. For the value  $f_F = 0.18$  appropriate to the  $\tau^+\tau^-$  annihilation mode in the sweet region, this ratio is equal to 1.30. For the value  $f_F = -0.09$  appropriate to the  $b\bar{b}$  annihilation mode in the sweet region, this ratio is equal to 0.9. Inserting either of these two  $f_F$  values into the ratios calculated with solar-matter effects, Eqs. (26)–(35), gives very different results.

We note that the change in flavor ratios over the transition from adiabatic ( $P_c^h = 0$ ) to nonadiabatic ( $P_c^h \rightarrow \cos^2 \theta_{13} \simeq 1$ ) is twice as large for the antineutrino sector in the inverted hierarchy, as compared to the neutrino sector in the normal hierarchy. This factor of two is subtle. We reveal its origin in the Appendix.

We may now use Eqs. (26)–(35) to obtain the magnitude of changes in the flavor ratios as the neutrino energy  $E$  varies across the sweet region. The energy-dependent  $P_c^h(E)$  is a monotonic function and obeys  $P_c^h(E \rightarrow 0) = 0$  and  $P_c^h(E \rightarrow \infty) = \cos^2 \theta_{13}$ . Thus, at leading order in  $\theta_{13}$  the range of the crossing probability is  $0 \lesssim P_c^h(E) \lesssim 1$ . We here list a sample of ratios of the quantities in Eqs. (26)–(35) above and below the adiabatic-to-nonadiabatic transition, calculated to order  $f_F^2$ , and then evaluated with the choices  $f_F = +0.18$  for the  $\tau^+\tau^-$  mode and  $f_F = -0.09$  for the  $b\bar{b}$  mode. In the normal hierarchy we have

$$\frac{\mathcal{R}_{P=1}^{\text{NH}}}{\mathcal{R}_{P=0}^{\text{NH}}} = 1 + \frac{9}{8}f_F + \frac{27}{32}f_F^2 = \begin{cases} 1 + 0.23 & (\tau^+\tau^-) \\ 1 - 0.09 & (b\bar{b}) \end{cases}, \quad (36)$$

$$\frac{(W_\mu^{\text{NH}}/W_e^{\text{NH}})_{P=1}}{(W_\mu^{\text{NH}}/W_e^{\text{NH}})_{P=0}} = 1 + \frac{9}{4}f_F + \frac{27}{16}f_F^2 = \begin{cases} 1 + 0.46 \\ 1 - 0.19 \end{cases}, \quad (37)$$

while in the inverted hierarchy we have

$$\frac{\mathcal{R}_{P=1}^{\text{IH}}}{\mathcal{R}_{P=0}^{\text{IH}}} = 1 + \frac{9}{4}f_F + \frac{189}{64}f_F^2 = \begin{cases} 1 + 0.50 & (\tau^+\tau^-) \\ 1 - 0.18 & (b\bar{b}) \end{cases}, \quad (38)$$

$$\frac{(\overline{W}_\mu^{\text{IH}}/\overline{W}_e^{\text{IH}})_{P=1}}{(\overline{W}_\mu^{\text{IH}}/\overline{W}_e^{\text{IH}})_{P=0}} = 1 + \frac{9}{2}f_F + \frac{81}{8}f_F^2 = \begin{cases} 1 + 1.14 \\ 1 - 0.32 \end{cases}. \quad (39)$$

The value of these ratios of ratios in vacuum is unity, of course. The large flavor-ratio differences here are due to the adiabatic-to-nonadiabatic transition at the matter-induced 2nd resonance. For the normal hierarchy, the ratio of ratios for the neutrino changes by 23% and 46% in the  $\tau^+\tau^-$  annihilation mode, and by 10% and 20% in the  $b\bar{b}$  mode. For the inverted hierarchy, the ratio of ratios for the antineutrino changes by slightly more than twice that, by 50% and 114% in the  $\tau^+\tau^-$  annihilation mode, and by 20% and 32% in the  $b\bar{b}$  mode. The changes for the two hierarchies are of opposite sign. Together with the very little change expected in the  $W^+W^-$  annihilation mode, one sees that just an inference of the existence and sign of the change can discriminate among the three most popular annihilation modes of solar WIMPs.

The qualitative factors for the change in the ratio of ratios, given in Eqs. (36)–(39), are borne out in the more exact results shown in Figs. 2–4.

## VI. DISCUSSION AND CONCLUSION

We have shown that

- For neutrinos from the  $\tau^+\tau^-$  annihilation mode of solar WIMPs, 10–100% changes in neutrino flavor ratios at Earth are expected in the 0.3–10 GeV energy interval. This energy interval is a mapping across the adiabatic-to-nonadiabatic transition of the higher-energy 2nd resonance in the Sun. Whether the change is 10% or 100%, or in between, depends on which flavor-ratio observable is available to the experimenter.
- For the  $b\bar{b}$  annihilation mode of the WIMPs, the flavor change is about half as large, and of opposite sign.
- For the  $W^+W^-$  annihilation mode, the flavor change is small.
- Arising from the higher-energy resonance in the Sun, the effect occurs in the neutrino sector but not antineutrino sector if the neutrino mass hierarchy is normal, and in the antineutrino but not neutrino sector if the mass hierarchy is inverted.
- Thus, a measurement of the sign and magnitude of this flavor change could indicate the WIMP annihilation mode, and a determination of the resonant sector, neutrino or antineutrino, would indicate the mass hierarchy.

A plot of flavor versus energy determines the energy  $E_{1/2}$  at which the adiabatic-to-nonadiabatic transition probability is 50% and determines the width (in energy)  $\Delta E$  of the transition. It turns out that

- $E_{1/2} \approx \Delta E$ , and each is proportional to  $\theta_{13}^2$ . Thus, the system is over-constrained, which provides a clean signal for the underlying physics.
- Moreover, the quadratic dependence on  $\theta_{13}$  provides a very sensitive probe for measuring the value of  $\theta_{13}$ .
- The adiabatic-to-nonadiabatic transition profile is measurable for  $\theta_{13}$  as small as  $0.5^\circ$ .

To establish experimentally a 30% change in the flavor ratios over the transition region with an  $n$ -sigma significance, the number of required CC  $\nu_e$  and  $\nu_\mu$  events is  $\sim 2(n/30\%)^2$ . (The pre-factor 2 arises from the need for statistical accuracy on each side of the transition.) Thus, for  $3\sigma$  significance one needs roughly 200 solar WIMP events separated from the atmospheric background and spanning the sweet region between 0.3 and 10 GeV. According to Eq. (8), a 200-event sample can be accumulated in the sweet region with a megaton detector in 1.5 years, if the WIMP annihilation cross section saturates its present experimental upper limit of  $3 \times 10^{-38} \text{cm}^2$ . The annihilation cross section could have this value, or it could be orders of magnitude less.

We end with mention of the many mega-detectors for low-energy neutrinos that have been proposed. They represent a presence of hope and vision that will shape the future. Proposed detector materials include water for Cerenkov signals (MEMPHYS, UNO, and HyperK), scintillators such as liquid argon (LENA, GLACIER, LArTPC, and T ASD), and magnetic iron calorimeters (MIND, MONOLITH, and INO). The magnetized detectors can distinguish neutrino and antineutrino events, which enhances the signal explored herein by a factor of two, and thereby reduces the data required by a factor of four. But magnetized detectors cannot be built as large as unmagnetized detectors.

### Acknowledgments

T.J.W. thanks Nicole Bell and the University of Melbourne for hospitality and support as well as Fido's Coffeehouse in Nashville, TN for a charming caffeine-rich writing environment. This work is supported in part by the DOE under Grant No. DE-FG05-85ER40226, by the European Commission under Grant No. MOIF-CT-2005-008687, and by CONACyT under Grant No. 55310.

### Appendix: The factor of two between antineutrino and neutrino adiabatic-to-nonadiabatic evolution

To explain the relative factor of two at order  $f_F$  between the neutrino's and the antineutrino's adiabatic-to-nonadiabatic evolution, we use the density-matrix formalism. In the flavor basis, the density matrix at Sun's core is  $\rho_F = \frac{1}{3} \mathbb{1} + f_F [2|\nu_\tau\rangle\langle\nu_\tau| - |\nu_\mu\rangle\langle\nu_\mu| - |\nu_e\rangle\langle\nu_e|]$ . Invoking the completeness relation  $\sum_\alpha |\nu_\alpha\rangle\langle\nu_\alpha| = \mathbb{1}$  as well as maximal neutrino mixing to symmetrize ( $2|\nu_\tau\rangle\langle\nu_\tau| - |\nu_\mu\rangle\langle\nu_\mu|$ )  $\rightarrow \frac{1}{2}(|\nu_\tau\rangle\langle\nu_\tau| + |\nu_\mu\rangle\langle\nu_\mu|)$  shows that this matrix may be rewritten in terms of just the  $\nu_e$  projector as  $\rho_F \rightarrow \frac{1}{3} [(1 + \frac{3}{2} f_F) \mathbb{1} - \frac{9}{2} f_F |\nu_e\rangle\langle\nu_e|]$ .

Now, with the normal hierarchy, and in the lower-energy adiabatic region, the  $\nu_e$  emerges from the Sun as  $\nu_3$ , and the  $\nu_\mu$  and  $\nu_\tau$  are left to emerge as  $\nu_1$  and  $\nu_2$ . In the higher-energy nonadiabatic region, the  $\nu_e$  emerges as  $\nu_2$ , while the  $\nu_\mu$  and  $\nu_\tau$  emerge as  $\nu_1$  and  $\nu_3$ . (Recall that we have chosen the sweet region to be below the nonadiabatic onset  $E_{NA}^l$  of the lower-energy 1st resonance, and so the conversion across the 1st resonance is  $\nu_e \leftrightarrow \nu_2$ .)

On the other hand, with the inverted hierarchy, and in the lower-energy adiabatic region, the  $\bar{\nu}_e$  again emerges as  $\bar{\nu}_3$  and the  $\bar{\nu}_\mu$  and  $\bar{\nu}_\tau$  emerge as  $\bar{\nu}_1$  and  $\bar{\nu}_2$ . However, in the higher-energy nonadiabatic region the  $\bar{\nu}_e$  emerges as  $\bar{\nu}_1$ , while the  $\bar{\nu}_\mu$  and  $\bar{\nu}_\tau$  are left to emerge as  $\bar{\nu}_1$  and  $\bar{\nu}_2$ .

Thus, at lower energies we have  $\nu_e \rightarrow \nu_3$  and  $\bar{\nu}_e \rightarrow \bar{\nu}_3$  in the normal and inverted hierarchies, respectively, while at higher energies we have  $\nu_e \rightarrow \nu_2$  and  $\bar{\nu}_e \rightarrow \bar{\nu}_1$  in the normal and inverted hierarchies, respectively. Replacing the  $\nu_e$  projector  $|\nu_e\rangle\langle\nu_e|$  in  $\rho_F$  with the appropriately evolved  $\nu$ -mass projector  $|\nu_1\rangle\langle\nu_1|$  or  $|\nu_2\rangle\langle\nu_2|$  or  $|\nu_3\rangle\langle\nu_3|$ , and then calculating the final flavor-matrix elements  $W_\mu = \langle\nu_\mu|\rho_F|\nu_\mu\rangle$  and  $W_e = \langle\nu_e|\rho_F|\nu_e\rangle$ , one readily obtains the change in flavor ratios ( $W_\mu/W_e$ ) across the adiabatic-to-nonadiabatic transition. To order  $f_F$ , the result is  $\frac{9}{2} f_F (\underline{U}_{e2} - \underline{U}_{\mu 2} + \underline{U}_{\mu 3} - \underline{U}_{e3})$  for the normal hierarchy, and  $\frac{9}{2} f_F (\underline{U}_{e1} - \underline{U}_{\mu 1} + \underline{U}_{\mu 3} - \underline{U}_{e3})$  for the inverted hierarchy. Putting into these expressions the values of tribimaximal mixing, one finds that the change is  $\frac{9}{4} f_F$  for the neutrino sector in the normal hierarchy, and twice that for the antineutrino sector in the inverted hierarchy. Notice that this result requires the mixing values of  $\nu_e$  and  $\nu_\mu$  with all three neutrino mass states. In the end, it is a "conspiracy" of the tribimaximal values that gives the seemingly simple factor of 2.

[1] R. Lehnert and T.J. Weiler, Phys. Rev. D **77**, 125004 (2008) [arXiv:0708.1035 [hep-ph]]; We note that in Ref. [6] it is stated that Ref. [1] analyzes solar neutrinos in the adiabatic approximation. This is incorrect:

in Ref. [1], both the adiabatic and nonadiabatic flavor evolution is studied in detail, and the adiabatic-to-nonadiabatic transition is delineated.

[2] The Borexino homepage is <http://borex.lngs.infn.it/>

- [3] The SNO+ homepage can be found at the URL <http://www.sno.phy.queensu.ca/group/projects.html>
- [4] We disregard the possibility of tau-neutrino regeneration, which would absorb high-energy neutrinos and re-inject them into the flux at lower energies. See also Footnote [13].
- [5] F. Halzen and D. Hooper, *New J. Phys.* **11**, 105019 (2009) [arXiv:0910.4513 [astro-ph.HE]]; T. Flacke, A. Menon, D. Hooper, and K. Freese, arXiv:0908.0899 [hep-ph]; V.D. Barger, W.Y. Keung, and G. Shaughnessy, *Phys. Lett. B* **664**, 190 (2008) [arXiv:0709.3301 [astro-ph]]; V.D. Barger, W.Y. Keung, G. Shaughnessy, and A. Tregre, *Phys. Rev. D* **76**, 095008 (2007) [arXiv:0708.1325 [hep-ph]]; F. Halzen and D. Hooper, *Phys. Rev. D* **73**, 123507 (2006) [arXiv:hep-ph/0510048]; S. Ritz and D. Seckel, *Nucl. Phys. B* **304**, 877 (1988).
- [6] J. Kumar, J.G. Learned, and S. Smith, *Phys. Rev. D* **80**, 113002 (2009) [arXiv:0908.1768 [hep-ph]].
- [7] V. Agrawal, T.K. Gaisser, P. Lipari, and T. Stanev, *Phys. Rev. D* **53**, 1314 (1996) [arXiv:hep-ph/9509423]; There also exist low-energy neutrino data. See, e.g., K. Daum *et al.* [Frejus Collaboration], *Z. Phys. C* **66**, 417 (1995).
- [8] S.J. Parke, *Phys. Rev. Lett.* **57**, 1275 (1986).
- [9] T.K. Kuo and J.T. Pantaleone, *Rev. Mod. Phys.* **61**, 937 (1989); *Phys. Rev. D* **39**, 1930 (1989).
- [10] For alternative analytical descriptions of neutrino propagation in matter, see, e.g., A.D. Supanitsky, J.C. D’Olivo, and G. Medina-Tanco, *Phys. Rev. D* **78**, 045024 (2008) [arXiv:0804.1105 [astro-ph]]; S.H. Chiu, T.K. Kuo, and L.X. Liu, arXiv:1001.1469 [hep-ph].
- [11] A. Esmaili and Y. Farzan, arXiv:0912.4033 [hep-ph]; M. Blennow, H. Melbeus, and T. Ohlsson, arXiv:0910.1588 [hep-ph]; A.E. Erkoca, M.H. Reno, and I. Sarcevic, *Phys. Rev. D* **80**, 043514 (2009) [arXiv:0906.4364 [hep-ph]]; M. Blennow, J. Edsjö, and T. Ohlsson, *JCAP* **0801**, 021 (2008) [arXiv:0709.3898 [hep-ph]].
- [12] M. Cirelli *et al.*, *Nucl. Phys. B* **727**, 99 (2005) [Erratum-ibid. B **790**, 338 (2008)] [arXiv:hep-ph/0506298].
- [13] For very heavy WIMP masses, the energy independence of flavor ratios will be affected by  $\nu_\tau$  “regeneration.” Neutrinos with energy above  $\sim 100$  GeV interact with the solar matter (the absorption probability is 60% at  $M_{\text{WIMP}} \simeq 200$  GeV). Via the CC interaction, the  $\nu_\tau$ ’s produce  $\tau$ ’s. Each  $\tau$  promptly decays to produce a lower-energy  $\nu_\tau$ . The cycle repeats, leading to a lower-energy flux of neutrinos, mostly  $\nu_\tau$ ’s. In general, this will contribute a calculable “secondary”  $E$ -dependence to the neutrino flavors in the sweet region.
- [14] The erratum in Ref. [12] corrects a programming error in their earlier paper that had suggested that the neutrino flavor ratio coming from the  $W^+W^-$  mode was energy independent, too. The earlier, erroneous energy-independent flavor ratio for  $W^+W^-$  was transcribed into Fig. 6 of Ref. [1].
- [15] We note that neutrinos are not appreciably absorbed in the Sun until their energies reach 50 GeV and above [1].
- [16] See, e.g., M.S. Athar *et al.* [INO Collaboration], “India-based Neutrino Observatory: Project Report. Volume I,” and references to earlier work therein; R. Gandhi *et al.*, *Phys. Rev. D* **76**, 073012 (2007) [arXiv:0707.1723 [hep-ph]].
- [17] W.H. Press and D.N. Spergel, *Astrophys. J.* **296**, 679 (1985); K. Griest and D. Seckel, *Nucl. Phys. B* **283**, 681 (1987) [Erratum-ibid. B **296**, 1034 (1988)]; A. Gould, *Astrophys. J.* **321**, 571 (1987); A.H.G. Peter, *Phys. Rev. D* **79**, 103532 (2009) [arXiv:0902.1347 [astro-ph.HE]].
- [18] S. Desai *et al.* [Super-Kamiokande Collaboration], *Phys. Rev. D* **70**, 083523 (2004) [Erratum-ibid. D **70**, 109901 (2004)] [arXiv:hep-ex/0404025].
- [19] R. Abbasi *et al.* [ICECUBE Collaboration], *Phys. Rev. Lett.* **102**, 201302 (2009) [arXiv:0902.2460 [astro-ph.CO]]; Earlier experiments with weaker limits on the solar  $\nu_\mu$  flux are M.M. Boliev *et al.* [Baksan Collaboration], *Nucl. Phys. B, Proc. Suppl.* **48**, 83 (1996); M. Ambrosio *et al.* [MACRO Collaboration], *Phys. Rev. D* **60**, 082002 (1999) [arXiv:hep-ex/9812020]; M. Ackermann *et al.* [AMANDA Collaboration], *Astropart. Phys.* **24**, 459 (2006) [arXiv:astro-ph/0508518].
- [20] We note that present limits on the spin-independent cross section of the WIMP are five orders of magnitude below that of the spin-dependent cross section. Such a huge ratio of the two cross-section types is a theoretical possibility, as this ratio depends sensitively on the nature of the WIMP.
- [21] Z. Ahmed *et al.* [CDMS Collaboration], *Phys. Rev. Lett.* **102**, 011301 (2009) [arXiv:0802.3530 [astro-ph]]; E. Behnke *et al.* [COUPP Collaboration], *Science* **319**, 933 (2008) [arXiv:0804.2886 [astro-ph]]; H.S. Lee *et al.* [KIMS Collaboration], *Phys. Rev. Lett.* **99**, 091301 (2007) [arXiv:0704.0423 [astro-ph]].
- [22] One might hope that the decay of the many pions produced in WIMP annihilation would enhance the flux of neutrinos at lower energies. However, the density of nucleons in the Sun’s core is  $n_N \sim 70 N_A/\text{cm}^3$ , and the pion interaction cross section is strong,  $\sigma_{\pi N} \sim 40$  mb. It follows that the mean interaction time is  $t_{\text{int}} = (cn_N \sigma_{\pi N})^{-1} \sim 2 \times 10^{-11}$  s. This is to be compared to the charged-pion lifetime of  $\tau_{\pi^\pm} = (E_\pi/m_\pi) \times 2 \times 10^{-7}$  s. Clearly, the pion loses energy and becomes innocuous through many subsequent absorptions and re-emissions, long before it can decay.
- [23] Reviews of possible very large detectors include D. Autiero *et al.*, *JCAP* **0711**, 011 (2007) [arXiv:0705.0116 [hep-ph]]; S. Choubey, arXiv:hep-ph/0609182.
- [24] J.G. Learned, arXiv:0902.4009 [hep-ex]; See also discussions in A. Bueno *et al.*, *JCAP* **0501**, 001 (2005) [arXiv:hep-ph/0410206]; O. Mena, S. Palomares-Ruiz, and S. Pascoli, *Phys. Lett. B* **664**, 92 (2008) [arXiv:0706.3909 [hep-ph]].
- [25] A. Bernstein *et al.*, arXiv:0908.4338 [nucl-ex].
- [26] J.E. Campagne, M. Maltoni, M. Mezzetto, and T. Schwetz, *JHEP* **0704**, 003 (2007) [arXiv:hep-ph/0603172]; P. Huber and T. Schwetz, *Phys. Lett. B* **669**, 294 (2008) [arXiv:0805.2019 [hep-ph]].
- [27] In the language of the matrices  $\underline{U}$ ,  $\underline{P}$ , and  $\underline{U}_m^T(0)$ , where  $\underline{P}$  is spelled out in Ref. [1], the flavor vectors can be expressed as follows:  $A_\alpha = 4 \underline{U} \underline{U}_m^T(0) (-1, -1, +2)^T$  and  $B_\alpha = 4 \underline{U} (\underline{P} - \mathbf{1}) \underline{U}_m^T(0) (-1, -1, +2)^T$ .
- [28] P.F. Harrison, D.H. Perkins, and W.G. Scott, *Phys. Lett. B* **530**, 167 (2002) [arXiv:hep-ph/0202074].
- [29] S. Pakvasa, W. Rodejohann, and T.J. Weiler, *Phys. Rev. Lett.* **100**, 111801 (2008) [arXiv:0711.0052 [hep-ph]].
- [30] M.C. Gonzalez-Garcia and M. Maltoni, *Phys. Rept.* **460**, 1 (2008) [arXiv:0704.1800 [hep-ph]].
- [31] M. Jacobson and T. Ohlsson, *Phys. Rev. D* **69**, 013003 (2004).